

## Reliable, High-Speed LEDs for Short-Haul Optical Data Links

By L. R. DAWSON, V. G. KERAMIDAS, and C. L. ZIPFEL

(Manuscript received August 31, 1979)

*A simple-geometry, broad-area (junction area extending over full area of chip), low-current density  $Ga_{1-x}Al_xAs$ -GaAs LED with exceptional light output stability has been developed for short-haul optical data link transmission. Electroluminescence rise and fall times are  $\sim 7$  and  $\sim 9$  ns, respectively, permitting data transmission rates as high as 32 Mb/s. At a current density of  $67 \text{ A/cm}^2$ , LED quantum efficiencies up to 3.5 percent (uncoated) are obtained. The spectral response peaks at  $8850 \text{ \AA}$ . At  $67 \text{ A/cm}^2$ , these LEDs launch in excess of  $30 \text{ }\mu\text{W}$  of optical power into butt-coupled fibers having a  $125\text{-}\mu\text{m}$  diameter core and 0.35 numerical aperture. The estimated failure rate for a 40-year service life is less than 1 FIT ( $<10^{-4}$  percent failures per 1000 hours).*

### I. INTRODUCTION

Recent advances in low-loss optical fibers have made optical fiber transmission systems one of the most promising new technologies. In a wide diversity of applications, different transmission distances and data transmission rates impose widely varying requirements in the design of fibers, light sources, detectors, and circuits used in conjunction with them.

For transmission rates in excess of  $\sim 30 \text{ Mb/s}$  over distances in excess of 5 km, high radiance sources, such as semiconductor lasers or long  $\lambda$  LEDs coupled to small-diameter, small numerical-aperture fibers are preferred. Such restrictions would be needed to guarantee suppression of pulse dispersion and to launch sufficient power into the fiber. There are, however, other applications which require lower transmission rates over distances less than a kilometer. Such requirements can be met with inexpensive, broad-area LEDs (junction area extending over full area of chip), used in conjunction with larger core-diameter, larger numerical-aperture fibers. In this paper, a low-current density LED is

described suitable for data transmission at rates as high as 32 Mb/s over distances less than 1 km. High reliability, simple geometry, low-current density operation and relative ease of fabrication make this LED an attractive choice for such applications. These devices have been used in a prototype system under test for use in electronic switching systems.<sup>1</sup>

## II. LED STRUCTURE

The LED structure is shown schematically in Fig. 1. It consists of a graded bandgap n-type  $\text{Ga}_{1-x}\text{Al}_x\text{As}$  layer and a p-type GaAs layer. A  $\text{Ga}_{1-x}\text{Al}_x\text{As}$ -GaAs heterostructure was chosen primarily to provide a low-loss radiation window for photons traveling toward the fiber. Under forward bias, carriers are injected predominantly from the wide energy gap  $\text{Ga}_{1-x}\text{Al}_x\text{As}$  region into the p-type GaAs region, where radiative recombination occurs, producing photons with energy near the energy gap of GaAs,  $\sim 1.4$  eV (8850Å). Photons emitted into the GaAs region are strongly absorbed, while the higher bandgap  $\text{Ga}_{1-x}\text{Al}_x\text{As}$  layer is an efficient window for light extraction.

The LED has been used with optical fibers having a  $\text{GeO}_2$ - $\text{SiO}_2$  core with  $\text{SiO}_2$  cladding. Such fibers are available with large core diameter (125  $\mu\text{m}$ ), large numerical aperture (0.35), and low loss at 8850.<sup>2</sup>

Ohmic contacts are made by evaporating 30 Å Al, 500 Å Sn, and 30,000 Å Au on the n-side and 800 Å of 1 w/o Be in Au and 2100 Å Au on the p-side with subsequent alloying.<sup>3</sup> The top contact configuration, shown in Fig. 1, consists of a solid field of metallization except for an essentially circular window 0.008-in. in diameter where the fiber is

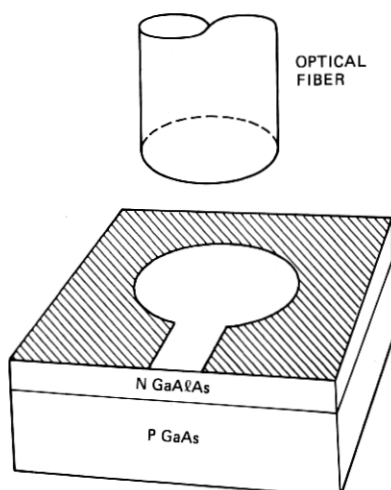


Fig. 1—Schematic of the broad-area optical data link LED.

ultimately placed close to the LED surface. This contact configuration maximizes current spreading from the metallized regions toward the center of the device where emitted light will enter the fiber. The bottom contact is full surface, resulting in a broad area LED.

Equally important to current spreading are the conductivity and thickness of the  $n\text{-Ga}_{1-x}\text{Al}_x\text{As}$  layer. The doping in this layer, however, is limited to modest levels by the need to keep the junction capacitance low. Excessive capacitance could limit the response speed of the LED. To maintain low capacitance, at least one side of the junction must have relatively low doping. Since the desire for high speed makes it imperative to highly dope the  $p\text{-GaAs}$  region (see below), there is no alternative to low doping on the  $n$ -side of the junction. The devices reported here have  $n$ -layers doped to a level of  $3 \times 10^{17} \text{ cm}^{-3}$ . For reasons discussed later, there are practical limitations to the thickness of the  $n$ -layer. The  $n$ -layers reported here are about  $30\text{-}\mu\text{m}$  thick. Doping density in the  $p$ -layer ranged from  $\sim 5 \times 10^{17}$  to  $>10^{19} \text{ cm}^{-3}$  to determine the optimum doping for optical power and high switching speed.

Final device geometry is achieved by sawing to give  $0.012 \times 0.012\text{-in.}$  square dice. Before mounting on TO-18 headers, the dice are etched in  $\text{HNO}_3$  to remove saw damage. The dice are mounted  $p$ -side down.

### III. MATERIAL PREPARATION

The LED structure shown in Fig. 1 is attained by first using liquid phase epitaxy (LPE) to grow sequentially an  $n\text{-Ga}_{1-x}\text{Al}_x\text{As}$  layer and a  $p\text{-GaAs}$  layer on a  $\text{GaAs}$  substrate, as shown in Fig. 2. After growth, the  $\text{GaAs}$  substrate is selectively removed from the epitaxial layers by a suitable chemical etch.<sup>4</sup> This procedure requires that these layers be thick enough to provide mechanical strength during processing.

This method of achieving the structure reported here is preferred to the somewhat more straightforward approach of first growing a  $p\text{-GaAs}$  layer and then the  $n\text{-Ga}_{1-x}\text{Al}_x\text{As}$  window layer, because of the considerable thickness required for the  $n$ -layer (see above). It is often difficult to completely remove the growth solution after the growth of such thick  $\text{Ga}_{1-x}\text{Al}_x\text{As}$  layers.

Growth is carried out in the sliding boat system shown in Fig. 3. The  $\text{Al}$  and  $\text{GaAs}$  source material to be used in Solution I is stored outside the melt during an initial oxide-removing bake at  $500^\circ\text{C}$ . This prevents the formation of significant amounts of  $\text{Al}_2\text{O}_3$  in growth Solution I, which could cause extensive mechanical difficulties during the growth process. After addition of the  $\text{Al}$  and  $\text{GaAs}$ , the system is equilibrated at  $920^\circ\text{C}$ . The approximate atom fraction composition of Solution I is  $X_{\text{Ga}}^I = 0.95$ ,  $X_{\text{As}}^I = 0.047$ ,  $X_{\text{Al}}^I = 0.0029$ ,  $X_{\text{Te}}^I = 0.000052$ . Solution II contains less  $\text{GaAs}$  than needed for  $\text{As}$  saturation at this temperature,

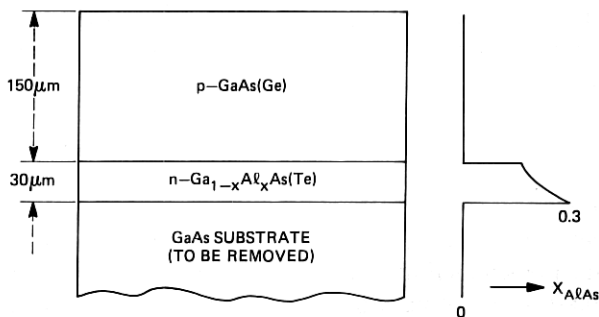


Fig. 2—Schematic representation of the epitaxial layers of the  $\text{Ga}_{1-x}\text{Al}_x\text{As}$ -GaAs LED showing dopants, layer thickness, and composition profile.

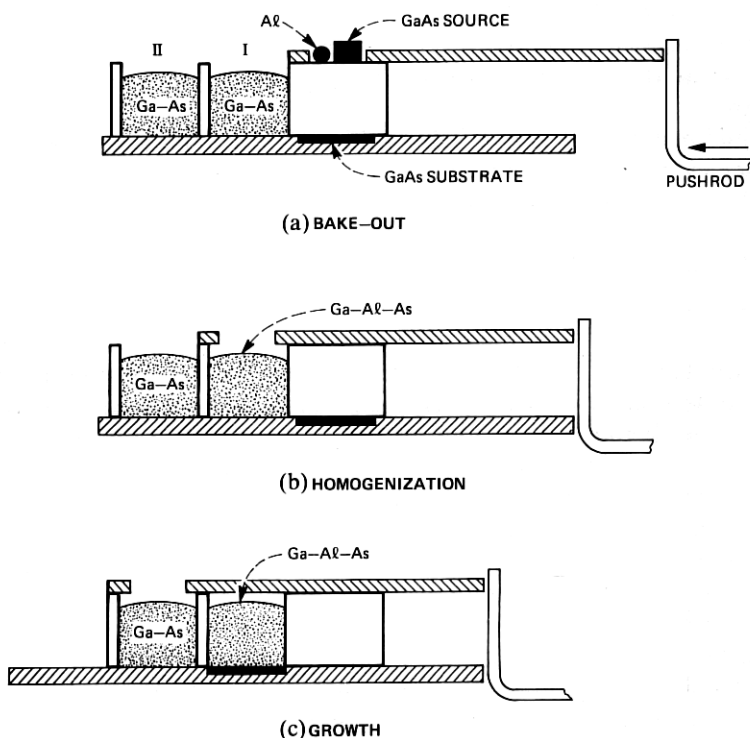


Fig. 3—Sliding boat system for the growth of the two-layer LED structure.

as discussed below, and the required amount of the Ge dopant. Growth is initiated by translation of the slider and the cooling of the system at a rate of  $0.4^\circ\text{C}/\text{min}$ . The liquid composition used results in  $\text{Ga}_{1-x}\text{Al}_x\text{As}$  layers whose initial value of  $x$  is  $\sim 0.3$ . Under these growth conditions,

Al segregates strongly in favor of the solid, leading to a decrease in  $x$  as growth proceeds due to depletion of Al from the bulk of the liquid. For very thick layers,  $x$  could decrease enough to increase optical absorption losses and/or reduce carrier injection into the GaAs region. To avoid such difficulties, the n-layers reported here are restricted to 30  $\mu\text{m}$  in thickness.

After the desired  $\text{Ga}_{1-x}\text{Al}_x\text{As}$  layer has been grown, usually during a period of 70 minutes, the slider is moved to bring the substrate in contact with Solution II. The amount of GaAs source dissolved earlier was chosen to bring the liquid close to the liquidus composition at this temperature,  $\sim 890^\circ\text{C}$ . Thus the substrate (on which an epitaxial layer has already been grown) contacts a solution which is close to equilibrium. Continued cooling causes growth of the GaAs layer. The liquid remains in contact with the substrate until room temperature is reached, resulting in GaAs layers 150  $\mu\text{m}$  thick. The total epitaxial growth is 180  $\mu\text{m}$ , which is thick enough to be handled without breakage after the substrate has been removed. For heavy Ge doping (discussed later), the last-to-grow material is often Ge rather than GaAs. Before processing, this Ge layer (which can be several mils thick) is lapped away.

The GaAs substrate is selectively removed using a preferential etch solution of  $\text{H}_2\text{O}_2$  (30 percent) whose pH has been adjusted to 8.5 with the addition of  $\text{NH}_4(\text{OH})$ .<sup>4</sup>

#### IV. DEVICE PERFORMANCE

For a current density of 67  $\text{A}/\text{cm}^2$ , LED external quantum efficiencies are typically 2.5 percent (uncoated) with a best value of 3.5 percent. Efficiency was found to be relatively insensitive to Ge doping level below  $p \approx 2 \times 10^{19} \text{ cm}^{-3}$ . However, the electroluminescent fall time  $\tau_f$  (90 to 10 percent peak output power) depends strongly on the hole concentration,  $p$ , in the GaAs recombination region. Figure 4 shows the dependence of  $\tau_f$  on  $X_{\text{Ge}}^{\text{I}}$ , the atomic fraction of Ge in the growth solution. The values of  $p$  shown were not measured but calculated from  $X_{\text{Ge}}^{\text{I}}$  and a knowledge of the distribution coefficient of Ge under similar growth conditions.<sup>5-7</sup> For  $p$  values in the range of  $5 \times 10^{17}$  to  $\sim 10^{19} \text{ cm}^{-3}$ , the power launched into the fiber remains essentially unchanged while  $\tau_f$  monotonically decreases from 300 to 9 ns. Increasing  $p$  beyond  $\sim 2 \times 10^{19} \text{ cm}^{-3}$  gives  $\tau_f$  values as low as 4 ns with an accompanying decrease in the power into the fiber. The solid line on this log-log plot was obtained by a least-squares fit to  $\ln \tau_f$  and  $\ln X_{\text{Ge}}^{\text{I}}$ . The slope of  $-1$  (correlation coefficient = 0.98) indicates  $\tau_f$  is inversely proportional to  $p$ . The deviation of the data for  $X_{\text{Ge}}^{\text{I}} > 10^{-1}$  may not be a departure from the  $p^{-1}$  proportionality, but may be an indication that Ge is not incorporated into the solid in the same

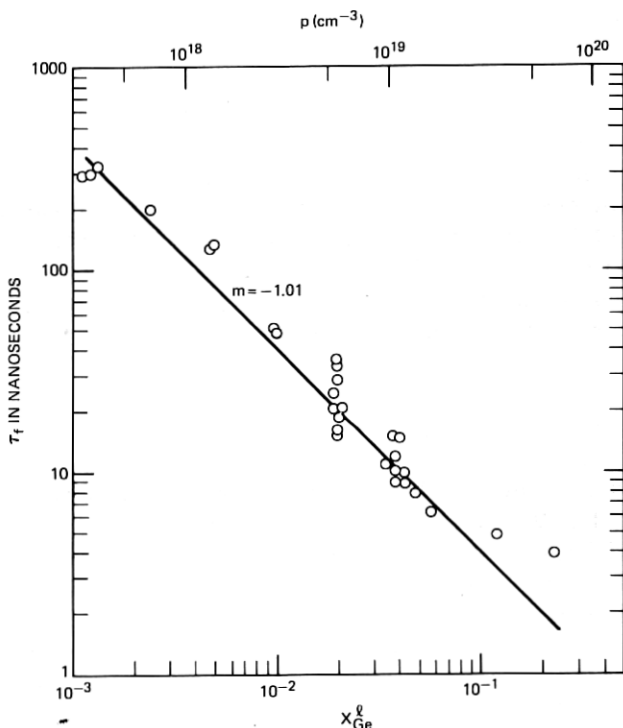


Fig. 4—Dependence of the electroluminescent fall time  $\tau_f$  on  $X_{Ge}^I$  (the atom fraction of Ge in the growth solution). Also shown are calculated values of the carrier concentration  $p$ .

manner at such high Ge concentrations in the liquid. For carrier concentration  $p \sim 2 \times 10^{19} \text{ cm}^{-3}$ , electroluminescent rise and fall times are typically 7 and 9 ns, respectively. The spectral emission of these LEDs peaks at  $8850 \text{ \AA}$  with a full width at half maximum of  $480 \text{ \AA}$ .

At a current density of  $67 \text{ A/cm}^2$ , these LEDs reproducibly launch in excess of  $30 \text{ \mu W}$  of optical power into optical fibers with a  $125\text{-}\mu\text{m}$  diameter core and a numerical aperture of 0.35. This power level is adequate for a number of applications including data transmission within electronic switching systems.<sup>1</sup>

## V. RELIABILITY

Accelerated aging tests at elevated temperatures are being performed on these devices to determine long-term stability. The LED chips being used in these tests are  $0.0165\text{-in.}$  square with a Ge concentration  $X_{Ge}^I = 3.2 \times 10^{-2}$ . The chips are mounted on TO-18 headers without encapsulation and are being aged at ambient temperatures of  $100^\circ$ ,  $150^\circ$ , and  $200^\circ\text{C}$ . Typical operating conditions for LEDs in an

optical data link are 60 mA forward current ( $34\text{A}/\text{cm}^2$  for these diodes) pulsed at 10 MHz at a maximum ambient temperature of  $60^\circ\text{C}$ . At the power dissipation under these conditions, the rise in junction temperature,  $T_J$ , is  $10^\circ\text{C}$  over the ambient. Ten diodes are being aged under each of the three following currents: (i) 60 mA at 10 MHz, (ii) 30 mA dc to compare with (i) and to determine whether there is enhanced degradation due to pulsing at the same average power dissipation, and (iii) 100 mA dc to determine the effect of increased current density.

Figure 5 shows the results of the accelerated aging studies at  $200^\circ\text{C}$ . There is a rapid initial degradation of a few percent in the first few hours of aging followed by very slow degradation. The degradation is somewhat enhanced as the stress current goes from 30 mA dc to 100 mA dc, in part due to the higher junction temperature at the higher current. If one takes into account the fact that the pulsed diodes are on only 50 percent of the time, they have degraded about 10 percent more than one would expect at 60 mA dc (by interpolating between the data for 30 mA dc and 100 mA dc). This effect is small, and may not be statistically significant. The diodes aged at  $100^\circ\text{C}$  and  $150^\circ\text{C}$  show only about 7 percent degradation after  $2 \times 10^4$  hours. The same tests have been performed on diodes from another wafer differing only in germanium concentration ( $X_{\text{Ge}}^1 = 1.8 \times 10^{-2}$ ) with essentially the same results.

As shown in Fig. 5, the data after about  $4.9 \times 10^3$  hours fall on a straight line when plotted as  $\log \eta/\eta_0$  versus  $t^{1/2}$ . Therefore, the

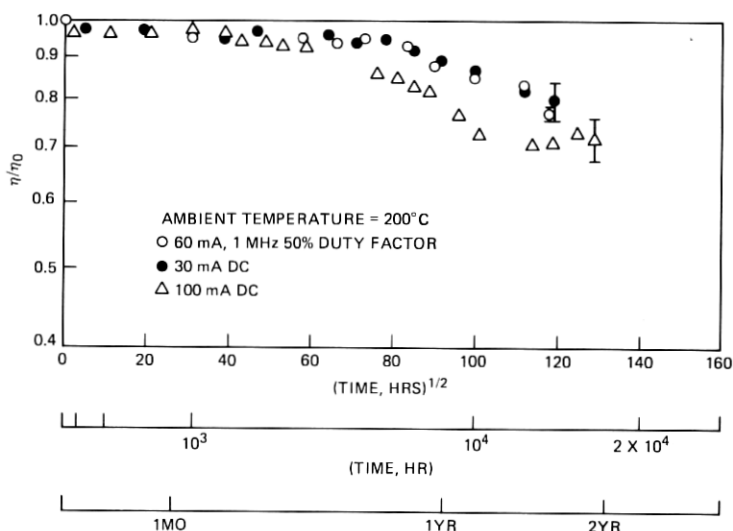


Fig. 5—Results of long-term aging at  $200^\circ\text{C}$  under various current conditions. The log of the relative degraded efficiency averaged for 10 diodes ( $\log \eta/\eta_0$ ) is plotted versus the square root of time.

degradation process can be described by

$$\eta/\eta_0 = \exp[-(t/\tau_{1/2})^{1/2}],$$

where  $\tau_{1/2}$  is a time constant for the degradation process and is approximately twice the -3 dB mean time to failure (MTTF). The data shown in Fig. 5 suggest that  $\tau_{1/2} = 8 \times 10^4$  hours (MTTF =  $4 \times 10^4$  hours) at  $T_J = 210^\circ\text{C}$ . The activation energy,  $E_A$ , for the slow degradation process is needed in order to estimate MTTF at the maximum anticipated operating temperature,  $T_J = 70^\circ\text{C}$ . There has not been sufficient degradation at the lower aging temperatures to allow the estimating of  $E_A$  for these devices. However, for diodes made from similar material and aged at a current density of  $670 \text{ A/cm}^2$ , an activation energy of 0.75 eV has been measured. Using this value, the MTTF at  $T_J = 70^\circ\text{C}$  is estimated to be  $7 \times 10^7$  hours.

It has been shown that LED failures resulting from a gradual degradation of light output follow lognormal statistics<sup>8</sup> with a failure distribution characterized by a standard deviation  $\sigma$  of less than unity. With MTTF =  $1 \times 10^8$  hours and  $\sigma = 1$ , the failure rate for a 40-year service life is estimated to be less than 1 FIT ( $10^{-4}$  percent failures per 1000 hours).<sup>9</sup>

## VI. ACKNOWLEDGMENTS

The authors express thanks to the late D. R. Ketchow for her assistance in the crystal growth, L. B. Hooker for the aging data, and W. H. Hackett, Jr. for response time and launched power measurements. We also wish to thank R. H. Saul and A. A. Bergh for numerous technical discussions and for their support.

## REFERENCES

1. W. H. Hackett, Jr., C. A. Bracket, L. E. Howarth, R. G. Smith, A. W. Warner, M. DiDomenico, Jr., and R. S. Riggs, Topical Meeting on Optical Fiber Transmission II, February 22-24, 1977, Williamsburg, Va.
2. W. G. French, J. B. MacChesney, P. B. O'Connor, and G. W. Tasker, "Optical Waveguides with Very Low Losses," B.S.T.J., 53, No. 5 (May-June 1974), pp. 951-954.
3. V. G. Keramidas, "GaAs and Related Compounds," Inst. Phys. Conf. Sec. No. 45, 396 (1978).
4. V. G. Keramidas, D. R. Ketchow, and F. Ermanis, unpublished results.
5. D. R. Ketchow, J. Electrochem. Soc., 121, No. 9 (1974), p. 1237.
6. F. E. Rosztochy, F. Ermanis, I. Hayashi, and B. Schwartz, J. Appl. Phys., 41, No. 1, (1970), p. 264.
7. F. E. Rosztochy and K. B. Wolfstirn, J. Appl. Phys., 42 (1971), p. 426.
8. R. H. Saul, E. H. Nicollian, D. A. Harrison, and F. Ermanis, unpublished results.
9. A. S. Jordan, Microelectronics and Reliability 18, No. 3 (1978), p. 267.